Effect of Parallel Flows and Toroidicity on Cross-Field Transport of Pellet Ablation Matter in Tokamak Plasmas

P. B. Parks[1,*] and L. R. Baylor[2]

[1]General Atomics, P.O. Box 85608, San Diego, California 92186-5608, USA

[2]Oak Ridge National Laboratory, Oak Ridge, Tennessee, USA

(Received 14 September 2004; published 1 April 2005)

The first complete set of time-dependent equations describing the cross-field drift of ionized pellet ablation matter in tokamak plasma caused by polarization in the nonuniform magnetic field has been developed and solved numerically. Important new features impacting the drift dynamics have been identified, including the effect of pressure profile variations in the tokamak plasma, curvature drive by near-sonic field-aligned (parallel) flows, and the rotational transform of the magnetic field lines, and are considered from the viewpoint of the parallel vorticity equation. These new features are necessary to obtain favorable quantitative agreement between theory and experimental fuel deposition profiles for both inner and outer wall launched pellet injection cases on the DIII-D tokamak.

DOI: 10.1103/PhysRevLett.94.125002 PACS numbers: 52.55.Fa

When a hydrogenic ice pellet immersed in a tokamak plasma is vaporized, a dense ionized ablation cloud is produced around the pellet [1]. The ionized part of the cloud has a pressure ~ 10 times higher than the surrounding plasma medium. The elevated pressure combined with the $1/R$ (R is the major radius) variation of the toroidal magnetic field induces an electric field, E, inside the ablated matter, propelling it across the magnetic field at the $E \times B$ drift velocity. Advection is in the direction of increasing R, thus making the usual injection from the outer wall, or high-R side of the torus, problematic: a large fraction $\sim 50\%$ of the pellet mass is simply expelled from the plasma. When pellets are injected from the inner wall side, the ablated pellet matter can be advected well past the distance penetrated by the pellet itself [2,3].

This Letter derives the first compete set of fully time-dependent equations describing the cross-field drift velocity of an ionized cloudlet $\vec{v}_{\perp c} = \{v_{\rho c}, v_{\chi c}\}$ with respect to the magnetic axis of a tokamak. We employ the plane polar coordinate system of a near circular, high-aspect-ratio toroidal plasma $\vec{\rho} = \{\rho, \chi\}$, where ρ is the radial (flux surface) label, χ the poloidal angle, $R = R_0 + \rho\cos\chi$, and R_0 is the major radius of the magnetic axis ($\rho = 0$). The new properties of the described model involve (1) enhanced curvature drive associated with near-sonic parallel flows, (2) incorporation of realistic (nonflat) plasma pressure profiles, (3) helical magnetic field line geometry (rotational transform), and (4) ''mass shedding'' caused by the disabling effect of magnetic shear on the lengthwise coherency of the $E \times B$ cloud drift. These new effects have not been addressed in previous theoretical models, which were of two basic variants: the ''continuous sheet stream'' model [4] and the ''discrete cloudlet'' model [5]. We build upon the latter approach. The supposition is that the pellet ablation process periodically forms a series of fully ionized, cylindrical ''cloudlets'' aligned along B. From this point on, we assume that the initial parameters of the cloudlets, radius r_c, half length L_c ($L_c \gg r_c$), density n_0, temperature T_0, pressure $p_0 = 2n_0T_0$, and sound speed $c_0 = (2T_0/m)^{1/2}$ (m is the ion mass), can be determined by the scaling laws of Ref. [5].

The two components of the transverse drift velocity require two equations. The first is derived from the generalized parallel vorticity equation [6],

$$\frac{\hat{b}}{B} \cdot \nabla \times mn \frac{d\vec{v}}{dt} = (\vec{B} \cdot \nabla)\frac{J_\parallel}{B} - \frac{(\hat{b} \times \vec{\kappa}) \cdot \nabla_\perp B^2}{\mu_0 B}. \quad (1)$$

Here $d/dt = \partial/\partial t + \vec{v} \cdot \nabla$, $J_\parallel$ is the density of parallel current, and $\vec{\kappa} = \hat{b} \cdot \nabla\hat{b}$ is the curvature of the magnetic field lines. The drifting cloudlet is *longitudinally expanding* while r_c remains fixed. It can be considered as a localized perturbation in pressure $\tilde{p} = p_c - p_\infty$ and flow velocity $\vec{v}$, where the subindex ∞ denotes a plasma equilibrium quantity. Though the initial cloudlet pressure $p_c = p_0$ can be almost an order of magnitude larger than p_∞, still $\beta_c = 2\mu_0 p_c/B_\infty^2 \ll 1$ [5]. Hence, the perturbed vorticity equation can be obtained by inserting the expanded quantities $J_\parallel = J_{\parallel\infty} + \tilde{J}_\parallel$ and $B^2 \cong B_\infty^2 + 2\vec{B}_\infty \cdot \vec{\tilde{B}}$ into Eq. (2), and then substituting $2\vec{B}_\infty \cdot \vec{\tilde{B}} = -2\mu_0\tilde{p}$ from the transverse force balance equation $0 \cong \nabla_\perp(\tilde{p} + \vec{B}_\infty \cdot \vec{\tilde{B}}/\mu_0) + O(\delta)$ where $\delta = r_c/R \ll 1$. Consequently, our first equation is

$$\frac{\hat{b}}{B} \cdot \nabla \times mn \frac{d\vec{v}}{dt} = (\vec{B} \cdot \nabla)\frac{\tilde{J}_\parallel}{B} - \frac{2(\hat{b} \times \vec{\kappa}) \cdot \nabla_\perp \tilde{p}}{\mu_0 B}. \quad (2)$$

The curvature of the field line is left unchanged by cloud perturbations to order δ. The second equation involves the divergence $\nabla \cdot \vec{v}_\perp = -2\vec{\kappa} \cdot \vec{v}_\perp$, which pertains, in general, to low-β, sub-Alfvénic transverse flows [7]. In this situation, the source term comes from the small compression in the transverse plane resulting from the velocity vectors $\vec{v}_\perp$ not all being parallel to each other along the

length of the *curved* cloud-field line. For low β, this can be rewritten as $\nabla \cdot \vec{v}_\perp = -(\vec{\kappa} + \nabla_\perp \ln B) \cdot \vec{v}_\perp$. This is a now a vector identity that holds for any vector of the form $\vec{v}_\perp = (\hat{b} \times \nabla\Phi)/B$, provided the scalar potential Φ obeys $\hat{b} \cdot \nabla\Phi = 0$. Comparing this form of $\vec{v}_\perp$ with the ideal MHD equation $\vec{E} + \vec{v}_\perp \times \vec{B} = 0$ indicates that the electric field driving transverse fluid motions in and near the cloudlet is dominantly electrostatic, $\vec{E} = -\nabla_\perp \Phi$. Since $\delta \ll 1$, the approximation $\nabla \cdot \vec{v}_\perp \cong 0$ provides the second equation.

Returning now to Eq. (2), we put $\vec{v} = v_\parallel \hat{b} + \vec{v}_\perp$, and $D/Dt = \partial/\partial t + \vec{v}_\perp \cdot \nabla_\perp$. The exact form of $d\vec{v}/dt$ reads

$$\frac{d\vec{v}}{dt} = \frac{D\vec{v}_\perp}{Dt} + \hat{b}\left[\frac{\partial v_\parallel}{\partial t} + v_\parallel \frac{\partial v_\parallel}{\partial s} + \vec{v}_\perp \cdot \nabla v_\parallel - v_\parallel(\vec{\kappa} \cdot \vec{v}_\perp)\right] + v_\parallel(\nabla \times \hat{b})_\parallel(\hat{b} \times \vec{v}_\perp) - v_\parallel \hat{b} \times \nabla \times \vec{v}_\perp + v_\parallel^2 \vec{\kappa}. \quad (3)$$

The last term is the centrifugal force in the curved magnetic field, and the last term in the parallel component is the corresponding Coriolis force. After inserting Eq. (3) into Eq. (2), we find that the centrifugal force term dominates. All other terms containing $v_\parallel$ are either smaller by order δ or do not contribute to the end results. Making the rearrangement $\hat{b} \cdot \nabla \times mnv_\parallel^2 \vec{\kappa} = -\hat{b} \times \vec{\kappa} \cdot \nabla_\perp (mnv_\parallel^2)$, we then obtain an equation for the evolution of the electrostatic potential,

$$\nabla_\perp \cdot \left(\frac{mn}{B^2}\frac{D\nabla_\perp \Phi}{Dt}\right) = (\vec{B} \cdot \nabla)\frac{\tilde{J}_\parallel}{B} + \frac{(\hat{b} \times \vec{\kappa}) \cdot \nabla_\perp (2\tilde{p} + mnv_\parallel^2)}{B}. \quad (4)$$

The heating and parallel expansion dynamics of the cloudlet is such that the centrifugal drive stemming from the parallel flow persists, even after the cloud pressure relaxes to the background pressure, $\tilde{p} \cong 0$. It is more convenient to evaluate the drive term in the reference frame moving with the cloudlet. Thus we introduce the local magnetic field line following the coordinate system $\{x, y, z\}$ or $\{r, \vartheta, z\}$, with $x = r\cos\vartheta$, $y = r\sin\vartheta$. Here $x = \text{const}$, $y = \text{const}$ labels a helical magnetic field line, and z is the distance along a field line coinciding with the cloudlet centroid ($x = 0, y = 0$). The orthogonal unit vectors $\hat{x} = \hat{\rho}$ and $\hat{y}$ point in the x and the y directions, i.e., normal to a magnetic surface and binormal to the field line. Any quantity $A(r, z)$ is assumed to be axisymmetric $\partial A/\partial\vartheta = 0$ and symmetric $A(r, z) = A(r, -z)$ about the midplane location ($z = 0$). Now let $\vec{\rho}_{c0}(t) = \{\rho_c(t), \chi_{c0}(t)\}$ be the instantaneous position of the cloudlet origin ($x = y = z = 0$), and let $\vec{\rho}_c(t) = \{\rho_c(t), \chi_c(t, z)\}$ designate the coordinate of a point somewhere along its centroid. Then $\chi_c(t, z) = \chi_{c0}(t) + z/q_c(t)R_0$, where $q_c(t) \equiv q[\rho_c(t)]$, and $2\pi/q(\rho)$ is the rotational transform of field lines. From a vector addition $\vec{\rho} = \vec{\rho}_c(t) + \vec{x}$, one readily derives

$$x = \rho\cos[\chi - \chi_c(t, z)] - \rho_c(t),$$
$$y = \rho\sin[\chi - \chi_c(t, z)]. \quad (5)$$

$$\hat{\rho} \cdot \hat{r} = \cos\vartheta\cos[\chi - \chi_c(z, t)] + \sin\vartheta\sin[\chi - \chi_c(z, t)], \quad (6a)$$
$$\hat{\chi} \cdot \hat{r} = \sin\vartheta\cos[\chi - \chi_c(z, t)] - \cos\vartheta\sin[\chi - \chi_c(z, t)]. \quad (6b)$$

With the usual approximation $\vec{\kappa} \cong -\hat{R}/R$, we obtain exactly $\hat{b} \times \hat{\kappa} \cdot \nabla_\perp = -[\sin\vartheta\cos\chi_c(z, t) + \cos\vartheta\sin\chi_c(z, t)]/R(\partial/\partial r)$ in Eq. (4). Hereafter, we treat R as a constant. Since Φ is independent of z, it can be solved for by annihilating the z dependence in Eq. (4) by an integration from $z = -L(t)$ to $L(t)$, giving

$$\nabla_\perp \cdot \vec{\Gamma} = \frac{-1}{BR}[\sin\vartheta\cos\chi_{c0}(t) + \cos\vartheta\sin\chi_{c0}(t)] \int_0^{L(t)} \frac{\partial}{\partial r} \times (2\tilde{p} + mnv_\parallel^2)\cos[z/q_c(t)R_0]dz. \quad (7)$$

The notation

$$\vec{\Gamma} = \frac{m\tau}{B^2}\left\{\frac{\partial\nabla_\perp\Phi}{\partial t} + (\vec{v}_\perp \cdot \nabla_\perp)\nabla_\perp\Phi\right\} + \frac{\nabla_\perp\Phi}{\mu_0 c_{A\infty}},$$
$$\tau(r, t) = \int_0^{L(t)} n(r, z, t)dz, \quad (8)$$

refers to, respectively, the line-averaged inertial (ion polarization) drift current and the column density. The last term in $\vec{\Gamma}$ comes from matching the parallel end current to the parallel current carried by outgoing shear-Alfvén waves in the background plasma with velocity $c_{A\infty}$, i.e., $\tilde{J}_\parallel(z = L) = -\nabla_\perp^2\Phi/(\mu_0 c_{A\infty})$ [5]. Because the *electrostatic* potential distribution carried along with the cloudlet moves from field line to field line relative to the background plasma, it acts like a source term for the Alfvénic *electromagnetic disturbance* that propagates out along the magnetic field lines. The presence of the $\cos(z/q_cR_0)$ factor in Eq. (7) stems from the rotational transform. As z increases, the grad-B drift current rotates *relative to the* $\{x, y\}$ *coordinates*. Toroidicity in this sense can become important if $L(t)$ grows to an appreciable fraction of the connection length $q\pi R_0/2$.

To find a closed form solution of Eq. (7) a "sharp boundary" cloudlet model may be assumed [5], with all quantities inside the cloud depending only on coordinate z: $n = [n_c(z, t) - n_\infty]H(r_c - r) + n_\infty$, $\tilde{p} + mnv_\parallel^2/2 = \{p_c(z, t)[1 + M_c^2/2] - p_\infty(t)\}H(r - r_c)$, where $M_c(z, t) = v_{\parallel c}/c$ is the cloud Mach velocity ($c^2 = p_c/mn_c = 2T_c/m$), and H is the unit step function. Inserting these expressions into Eq. (7) one gets

$$\nabla_\perp \cdot \vec{\Gamma} = \frac{2}{BR}\delta(r - r_c)[\sin\vartheta\cos\chi_{c0}(t) + \cos\vartheta\sin\chi_{c0}(t)]\Psi(t). \quad (9)$$

The "toroidal drive integral

$$\Psi(t) = \int_0^{L(t)} [p_c(t,z) - p_\infty(t) + M_c^2(z,t)] \times \cos[z/q(t)R] dz \tag{10}$$

captures the effect of realistic (nonuniform) plasma profiles, $p_\infty(t) \equiv p_\infty[\rho_c(t)]$, although n_∞ is considered uniform. The background pressure (temperature) profile can seriously limit cloud penetration depth for inboard pellet injection compared to previous model calculations [4,5] since the cloud is drifting from the plasma edge up the pressure gradient, reducing Ψ. To evaluate Ψ, the pressure and velocity evolution along B is obtained from the 1D Lagrangian fluid code [5]. Parallel evolution is influenced by the drift in the present model because both the heating rate by incident plasma electrons and the boundary condition at the cloud-plasma contact surface, $p_c[z = L(t), t] = p_\infty(t)$, become time dependent.

The divergence term $\nabla_\perp \cdot \vec{\Gamma}$ in Eq. (9) is then evaluated separately for $r < r_c$ and for $r > r_c$. First, employ $\nabla \cdot \vec{v}_\perp = 0$ to obtain the relation $\nabla_\perp \cdot [(\vec{v}_\perp \cdot \nabla_\perp)\nabla_\perp \Phi] = \vec{v}_\perp \cdot \nabla_\perp (\nabla_\perp^2 \Phi)$. Then, because $\nabla_\perp \tau = 0$ for $r \neq r_c$, we get for $r \neq r_c$

$$\nabla_\perp \cdot \vec{\Gamma} = \left\{ \frac{m\tau}{B^2} \left(\frac{\partial}{\partial t} + \vec{v}_\perp \cdot \nabla_\perp \right) + \frac{1}{\mu_0 c_{A\infty}} \right\} \nabla_\perp^2 \Phi = 0. \tag{11}$$

Thus, at any arbitrary instant, the electrostatic potential obeys Poisson's equation $\nabla_\perp^2 \Phi = 0$ in each region. After employing continuity of F at $r = r_c$, the potential in the tokamak frame (but expressed using cloud frame coordinates) reads $\Phi = \Phi_{\rm in}$ ($\Phi_{\rm out}$) for $r < r_c$ ($> r_c$) with

$$\begin{aligned} \Phi_{\rm in} &= C(t) y + [D(t) - E_{\rho\infty}(t)] x, \\ \Phi_{\rm out} &= C(t) \frac{r_c^2}{r} \sin\vartheta + D(t) \frac{r_c^2}{r} \cos\vartheta - E_{\rho\infty}(t) x. \end{aligned} \tag{12}$$

The boundary condition at $r \to \infty$ was predicated on the assumption that the background tokamak radial electric field changes slowly on the scale of the cloud dimensions, so it can be written as $E_{\rho\infty}(t) \equiv E_{\rho\infty}[\rho_c(t)]$. The potential represents the superposition of two mutually orthogonal dipoles, with dipole constants C and D that are clearly related to the time-dependent cloud (or centroid origin) velocity components $C = -v_{\rho c} B$, $D = \mathrm{v}_{\chi c0} B + E_{\rho\infty}(\rho_c)$, in which $v_{\chi c0}(t) = \rho_c(t) \partial \chi_{c0}(t)/\partial t$ and $v_{\rho c}(t) = \partial \rho_c(t)/\partial t$. To resolve the dipole constants, we first apply the divergence theorem to Eq. (9), getting

$$\hat{r} \cdot (\vec{\Gamma}|_{r_c+\varepsilon} - \vec{\Gamma}|_{r_c-\varepsilon}) = \frac{2}{BR} [\sin\vartheta \cos\chi_{c0}(t) + \cos\vartheta \sin\chi_{c0}(t)] \Psi(t). \tag{13}$$

Since the background plasma behaves as an inertia-free medium, $n_\infty \sim (10^{-3}\text{–}10^{-4}) n_c$, we may write for the left side of Eq. (13)

$$\frac{\hat{r} \cdot [\nabla_\perp \Phi_{\rm out} - \nabla_\perp \Phi_{\rm in}]|_{r=r_c}}{\mu_0 c_{A\infty}} - \frac{m\tau_{\rm in}(t)}{B^2} \hat{r} \cdot \left\{ \frac{\partial}{\partial t} \nabla_\perp \Phi_{\rm in} + (\vec{v}_{\perp \rm in} \cdot \nabla_\perp \nabla_\perp \Phi_{\rm in}) \right\} \Big|_{r=r_c}, \tag{14}$$

in which gradient and time operators are evaluated in the fixed tokamak frame of reference, with the exception of the first term involving Alfvén wave emission, where the difference in the radial electric field across the cloud boundary, i.e., the surface charge density is frame invariant. For convenience, we evaluate this term by direct substitution of Eq. (12), keeping cloud frame coordinates. To evaluate the second and third terms in Eq. (14) we have to first replace the cloud coordinates in $\Phi_{\rm in}$ by means of Eqs. (5), then use Eqs. (6). The third nonlinear convective term is identically zero; remarkably, the nonlinear contribution, to be discussed shortly, comes from the second term. Equating the $\sin\vartheta$ and $\cos\vartheta$ components on both sides of Eq. (13) leads to two equations for C and D, which translates into two equations for the radial and poloidal cloud centroid drift velocities. Using rescaled variables, $\tilde{t} = t/(L_c/c_0)$, $v_\rho = v_{\rho c}/c_0$, $v_\chi = v_{\chi c0}/c_0$, $v'_\chi = v_{\chi c}/c_0$ [$\mathrm{v}_{\chi c} = \rho_c(t) \partial \chi_c(t,z)/\partial t$], the equations in nondimensional form read

$$M(\tilde{t}) \frac{dv_\rho}{d\tilde{t}} = -\nu_A v_\rho + g\tilde{\Psi}(\tilde{t}) \cos\chi_{c0}(\tilde{t}) + wM(\tilde{t}) \frac{v_\chi v'_\chi}{\tilde{\rho}_c}, \tag{15a}$$

$$M(\tilde{t}) \frac{dv_\chi}{d\tilde{t}} = -\nu_A [v_\chi - v_E(\tilde{\rho}_c)] - g\tilde{\Psi}(\tilde{t}) \sin\chi_{c0}(\tilde{t}) - wM(\tilde{t}) \frac{v_\rho v'_\chi}{\tilde{\rho}_c}, \tag{15b}$$

with $d\tilde{\rho}_c/dt = w v_\rho$. The other normalized quantities are defined as $\tilde{\rho}_c = \rho_c/a$, $w = L_c/a$, $\tilde{\Psi} = \Psi/p_0 L_c$, $g = 2L_c/\tilde{\tau}R$, $\tilde{\tau} = \tau_{\rm in}(0)/n_0 L_c(\sim 1)$, $M = \tau_{\rm in}(t)/\tau_{\rm in}(0)$, and v_E is the normalized plasma $E_{\rho\infty} \times B$ convective velocity. It is important to not confuse v_E with the plasma *poloidal rotation velocity,* which can be quite different in a torus. The dimensionless damping coefficient associated with Alfvén wave emission is $\nu_A = (2/\tilde{\tau})(n_\infty/n_0)(c_{A\infty}/c_0)$. Alfvén wave emission discharges the polarization charges and exchanges momentum between the two media. If there is no *relative* motion between the $E_{\rho\infty} \times B$ flow and the cloud drift, there are no polarization charges and no momentum exchange is possible. The nonlinear velocity terms appearing in Eqs. (15) come from the polarization current generated by the centrifugal and Coriolis forces acting on a cloud brought into poloidal rotation either by spin up or by simply launching the pellet off the midplane, making $\sin\chi_{c0}(t)$ in Eq. (15b) nonzero at $t = 0$. Now $v'_\chi = v_\chi$ in the absence of magnetic shear. However, with finite magnetic shear a small differential drift (in the poloidal direc-

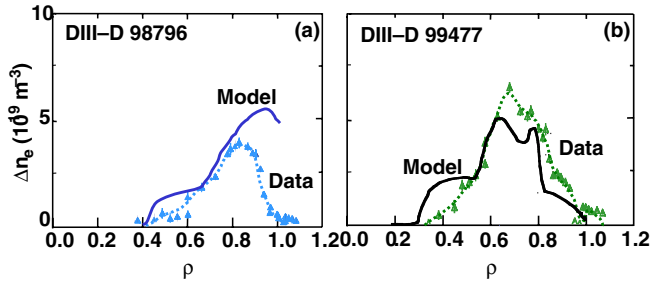

FIG. 1 (color online). (a) Fuel mass deposition profile Δn from a 2.7 mm cylindrical deuterium pellet (equivalent spherical radius 1.54 mm) injected at 586 m/s from the outer wall midplane of DIII-D, $\chi_{c0}(0) = 0$. (b) Δn for a similar pellet injected at 153 m/s from the inner wall of DIII-D, 35 cm above the midplane, $\chi_{c0}(0) \approx 3\pi/4$.

tion only) develops along the length of the cloudlet, with magnitude given by $\delta v_\chi \equiv v'_\chi - v_\chi = (\rho_c z/c_0 R_0)\partial(1/q_c)/\partial t = v_\rho z/L_s$. Here $L_s = qR_0/\hat{s}$ is the magnetic shear scale length, and $\hat{s} = (\rho/q)(dq/d\rho)$ is the shear parameter. We assumed from the outset that field lines in a flux tube could be labeled by the coordinates (x, y), implying the absence of shear. When shear is nonzero, the field lines should be labeled by the "twisted basis" coordinates (x_*, y_*), where $x_* = x$, $y_* = y - xz/L_s$. Then an alternate way to derive the correction δv_χ can be found by simply mapping the coordinates in our *shear-free* solution: $\Phi_{\rm in}(x, y) \rightarrow \Phi_{\rm in}(x_*, y_*)$. For this representation, $\partial\Phi_{\rm in}/\partial x = \partial\Phi_{\rm in}/\partial x_* - (z/L_s)\partial\Phi_{\rm in}/\partial y_*$, $\partial\Phi_{\rm in}/\partial y = \partial\Phi_{\rm in}/\partial y_*$. Then $\vec{v}_{\perp \rm in} = \hat{z} \times \nabla\Phi_{\rm in}/B_\infty$ reproduces the above result, namely, $\vec{v}_{\perp \rm in}/c_0 = \{v_\rho, v_\chi + \delta v_\chi\}$. The reason for the z dependence in δv_χ is due to the shear-induced twist in flux tube–cloud cross section, gradually changing the cloud boundary from a circle, $r = r_c$ at $z = 0$, into a rotated ellipse, $x^2(1 + z^2/L_s^2) + 2xy(z/L_s) + y^2 = r_c^2$. Geometric distortion brings the space charge layers closer together in the x direction as z increases, resulting in a differential drift in the y (or the χ) direction only. The main effect of shear is that it causes loss of coherency by shifting the end parts of the cloud to flux tubes outside the influence of the electrostatic fields when the centroid of those parts shifts by the amount $\sim 2r_c$ with respect to cloud origin $z = 0$. Then those fluid elements are unable to participate in the coherent drift motion and stop drifting with the rest of the cloudlet. Beginning with the outermost elements, they sequentially peel off one by one and get deposited in the plasma almost immediately: because of their small relative mass ($\delta M \ll M$) the residual Alfvén drag "coasting distance" is extremely small. An *ad hoc* prescription for the "shedding time" $t_s(z_0)$ of a fluid element with the initial Lagrangian coordinate z_0 reads (in dimensional variables)

$$2r_c = \int_0^{t_s(z_0)} \frac{v_{\rho c}(t) z(z_0, t) dt}{L_s[\rho_c(t)]}, \tag{16}$$

where $z(z_0, t)$ is its later position. The mass loss rate is $dM/dt = -(dM/dz_0)(dz_0/dt_s)$. Low magnetic shear (large L_s) favors deeper fuel penetration because it delays shedding and fuel dispersal. Of course, any mass remaining in the cloudlet when it does finally come to a full stop, by the combination of Alfvén wave emission and reduced toroidal drive Ψ, is locally deposited at the stopping point. The fuel deposition profile Δn, may then be constructed by summing over the deposition profile from each cloudlet produced by a single pellet.

The calculated deposition profile Δn for outer wall midplane, $\chi_{c0}(0) = 0$, and inner wall above-midplane $\chi_{c0}(0) \approx 3\pi/4$ pellet injection cases on DIII-D are shown by the solid curves in Fig. 1, respectively. The experimental Δn recorded by Thomson scattering ($\Delta n = \Delta n_e$) less than 1 ms after the pellet ablates [3] is overlaid (dashed curve). In both cases the present theory compares well with the experimental data. However, in the outer wall injection case the experimental profile begins to deviate sharply from the calculated one near the edge, i.e., for $\rho/a > 0.85$. The profile discrepancy is likely due to a strong edge localized mode (ELM) triggered during the pellet injection event, which causes a large fraction of the edge pedestal density to be expelled from the plasma [3]. This is also consistent with the modest discrepancy between the experimental and calculated particle fueling efficiencies, 46% versus 66%, respectively. For inner wall injection, the triggered ELM is much less pronounced: both measured and calculated fueling efficiencies are practically 100%.

This work was supported by the U.S. Department of Energy under Grants No. DE-FC02-04ER54698, No. DE-FG03-95ER54309, and No. DE-AC05-00OR22725.

*Electronic address: parks@fusion.gat.com

[1] R. Ishizaki, P. B. Parks, N. Nakajima, and M. Okamoto, Phys. Plasmas **11**, 4064 (2004). (Also see references therein.)
[2] P. T. Lang *et al.*, Nucl. Fusion **40**, 245 (2000).
[3] L. R. Baylor *et al.*, Phys. Plasmas **7**, 1878 (2000).
[4] V. Rozhansky, I. Senichenkov, I. Veselova, and R. Schneider, Plasma Phys. Controlled Fusion **46**, 575 (2004).
[5] P. B. Parks, W. D. Sessions, and L. R. Baylor, Phys. Plasmas **7**, 1968 (2000).
[6] R. D. Hazeltine and J. D. Meiss, *Plasma Confinement* (Addison-Wesley, Reading, MA, 2003), ISBN 0-486-43242-4.
[7] J. F. Drake and T. M. Antonsen, Jr., Phys. Fluids **27**, 898 (1984).